Environmental Pollution 289 (2021) 117974

Contents lists available at ScienceDirect

Environmental Pollution

journal homepage: www.elsevier.com/locate/envpol

Long-term variability in base cation, sulfur and nitrogen deposition and critical load exceedance of terrestrial ecosystems in China☆

Wenxin Zhao [a], Yu Zhao [a,b,*], Mingrui Ma [a,c], Ming Chang [c], Lei Duan [d]

[a] State Key Laboratory of Pollution Control & Resource Reuse and School of the Environment, Nanjing University, Nanjing, Jiangsu, 210023, China
[b] Jiangsu Collaborative Innovation Center of Atmospheric Environment and Equipment Technology (CICAEET), Nanjing University of Information Science & Technology, Nanjing, Jiangsu, 210044, China
[c] Institute for Environmental and Climate Research, Jinan University, Guangzhou, Guangdong, 511486, China
[d] School of Environment, Tsinghua University, Beijing, 100084, China

ARTICLE INFO

Keywords:
Atmospheric deposition
Critical load
Interannual change
Acidification

ABSTRACT

The rapid development of China's industrial economy and implementation of air pollution controls have led to great changes in sulfur (S), nitrogen (N) and base cation (BC) deposition in the past three decades. We estimated China's anthropogenic BC emissions and simulated BC deposition from 1985 to 2015 with a five-year interval using a multilayer Eulerian model. Deposition of S and N from 2000 to 2015 with a five-year interval was simulated with the EMEP MSC-W model and the Multi-resolution Emission Inventory of China (MEIC). The critical load (CL) and its exceedance were then calculated to evaluate the potential long-term acidification risks. From 1985 to 2005, the BC deposition in China was estimated to have increased by 16 % and then decreased by 33 % till 2015. S deposition was simulated to increase by 49 % from 2000 to 2005 and then decrease by 44 % in 2015, while N deposition increased by 32 % from 2000 to 2010 with a limited reduction afterward. The maximum CL of S was found to increase in 67 % of mainland China areas from 1985 to 2005 and to decline in 55 % of the areas from 2005 to 2015, attributed largely to the changed BC deposition. Consistent with the progress of national controls on SO_2 and NO_X emissions, the CL exceedance of S increased from 2.9 to 4.6 Mt during 2000–2005 and then decreased to 2.5 Mt in 2015, while that of N increased from 0.4 in 2000 to 1.2 Mt in 2010 and then decreased to 1.1 Mt in 2015. The reduced BC deposition due to particle emission controls partially offset the benefit of SO_2 control on acidification risk reduction in the past decade. It demonstrates the need for a comprehensive strategy for multi-pollutant control against soil acidification.

1. Introduction

Atmospheric deposition of sulfur (S) and nitrogen (N) elevates the acidification and eutrophication risks of terrestrial ecosystems (Burns et al., 2016; Payne et al., 2011; Zhang et al., 2018a). China has become the dominant sources of sulfur dioxide (SO_2) and nitrogen oxides (NO_X) in Asia and has experienced abundant acid deposition, with national average precipitation pH levels fluctuating between 4.6 and 5.6 during 1980–2014 (Yu et al., 2017, 2020). The country has been implementing a series of measures to control air pollutant emissions since 2005, including the application of flue gas desulfurization (FGD) and selective catalytic reduction (SCR) systems in selected industries for SO_2 and NO_X control, respectively. These measures have been proven to be successful. As indicated by the Multi-resolution Emission Inventory for China (MEIC, http://www.meicmodel.org), the national SO_2 and NO_X emissions started to decline after 2007 and 2012, respectively (Li et al., 2017; Liu et al., 2015). With the growth in agricultural activities, in contrast, a 2.4-fold increase in ammonia (NH_3) emissions was estimated from 1980 to 2016 (Fu et al., 2020).

Besides S an N, the base cations (BCs) in particulate matter (PM) of natural and anthropogenic origins play an important role on neutralizing acid deposition (Fenn et al., 2015). The steep reduction in BC concentrations was found to greatly decrease the benefit of S and N controls on reducing precipitation acidity in Europe and the United State (the U.S.) (Cecchini et al., 2019; Jeziorski and Smol, 2017; McHale et al., 2017; Meesenburg et al., 2016). Due to the high levels of industrial

☆ This paper has been recommended for acceptance by Admir C. Targino.

* Corresponding author. State Key Laboratory of Pollution Control & Resource Reuse and School of the Environment, Nanjing University, Nanjing, Jiangsu, 210023, China.
E-mail address: yuzhao@nju.edu.cn (Y. Zhao).

https://doi.org/10.1016/j.envpol.2021.117974
Received 24 September 2020; Received in revised form 4 July 2021; Accepted 12 August 2021
Available online 14 August 2021

production and coal consumption, the PM and BC emissions of anthropogenic origin in China were much higher than those in developed European countries and in the U.S., resulting in more significant impact on acidification risk, particularly in Southeast and Southwest China (Crippa et al., 2018; Klimont et al., 2017; Posch et al., 2015). Based on the monitored wet BC deposition data, Zhang et al. (2020) applied an area-weighted method and estimated BC deposition at the national scale for China. They found that the wet BC deposition experienced a decreasing trend from 2000 to 2017 and buffered 85 % of precipitation acidity caused by SO_4^{2-} and NO_3^-. However, the insufficient sites and lack of dry deposition observations caused the assessment of the acid neutralization of BCs to be incomplete. Chemistry transport models (CTMs) that combine emission data and meteorology have also been applied to illustrate the spatial and temporal patterns of BC deposition (Draaijers et al., 1997; Duan et al., 2007; Larssen and Carmichael, 2000). The rapid economic development, adjusted industrial structure, and stricter air pollution controls have jointly resulted in significant changes in emissions and deposition of anthropogenic BCs (Li et al., 2017; Zhang et al., 2019).

Till now, the long-term evolution of acidification risks due to the changed deposition of multiple pollutants has been insufficiently explored for China. In particular, the long-term changes in BCs have seldom been combined with those of S and N to evaluate the comprehensive effects of multi-pollutant control on ecosystem acidification. Compared to SO_2, the studies on long-term trend of BC emissions were still lacking for China. For example, Ministry of Ecology and Environment of China (MEE) started to report the national annual SO_2 emissions in 1985 (MEE, 2020), but very limited emission data were available for BCs. Given the importance of balance between anions and cations, the long-term trends in BC emissions and deposition need to be fully evaluated.

As an indicator of the sensitivity of terrestrial ecosystems to acidification and eutrophication, critical load (CL) has been widely applied to determine the threshold for acid deposition without irreversible ecosystem damage. This concept considers the heterogeneity of vegetation, soil, meteorology and BC deposition by region and makes full use of the buffering capacity of ecosystems (UNECE, 2004). CL has been widely estimated in different regions, including Europe (Posch et al., 2015), the U.S. (Nanus et al., 2012; Pardo et al., 2011), and Asia (Reinds et al., 2008). The CL and its exceedance have been calculated and mapped to indicate the ecological risks and emission reduction goals for Europe (Hettelingh et al., 2013; Posch et al., 2015; Reis et al., 2012) and China (Duan et al., 2000; Jia and Gao, 2017). However, the effects of decadal environmental changes (e.g., variations in BC deposition due to changed emissions, and those in soil weathering rate due to changed temperatures) on the CL have seldom been analyzed. Furthermore, there is limited analysis of spatiotemporal variations in CL exceedance on a long-term scale, thus the effectiveness of emission controls on soil acidification recovery remains unclear.

In response to the above limitations, this study aimed to develop an integrated modeling framework for the long-term variability of multi-pollutant (BCs, S and N) deposition and to explore the comprehensive effects of the national policy of air pollution controls on soil acidification for decades in China. We developed an emission inventory of China's anthropogenic BCs from 1985 to 2015 with a five-year interval and simulated the annual deposition with a multilayer Euler model. We integrated the long-term changes in BC deposition and meteorological conditions, and quantified the interannual variations in the CL. Based on the MEIC emission data, we applied the EMEP MSC-W model to simulate the S and N deposition from 2000 to 2015 with a five-year interval. By comparing the simulated acid deposition and CL, we calculated corresponding CL exceedance of terrestrial ecosystems across the country to reveal the effectiveness of multi-pollutant controls on reducing soil acidification risks. The case of China serves a profound demonstration of national air pollution control and environmental damage alleviation, and provides policy guidance for countries at the similar development stage.

2. Material and methods

2.1. Emission inventory of BCs

We estimated the calcium (Ca) and magnesium (Mg) emissions of anthropogenic origin for China from 1985 to 2015 with a five-year interval (i.e., 1985, 1990, 1995, 2000, 2005, and 2015) based on PM emissions and the mass fractions of Ca and Mg in PM. Potassium and sodium were not included due to their very small shares of BC emissions). The 31 provinces in mainland China were included. The emission sources contained six major categories, i.e., power generation, cement production, iron & steel production, industrial boilers, other industrial processes, and residential coal combustion. The annual emissions were calculated by province and sector with Eq. (1):

$$Q_{i,t} = \sum_{j,k} Q_{P,\,j,k,t}\; w_{i,j,k} \tag{1}$$

where Q_P is the PM emissions; w is the percentage of BCs to the total PM emissions by mass; and i, j, k and t represent the BC species, province, sector and year, respectively.

Two PM emission inventories were used in calculating BC emissions. PM emissions from 1985 to 1995 were obtained from the Emission Database for Global Atmospheric Research version 4.3.2 (EDGAR) released by the European Commission Joint Research Center (Crippa et al., 2018). For 2000–2015, we applied a emission inventory developed in our previous work (Xia et al., 2016). With a "bottom-up" methodology, this inventory incorporated the available data from large point sources (e.g., power and cement plants) and tracked the interannual changes in the PM emission factors attributed to the improved application of dust collectors. Since EDGAR did not report total PM but PM_{10} (PM with aerodynamic diameters less than 10 μm), we used the PM_{10} emissions in EDGAR and the mass fractions of PM_{10} to PM for 2010 in Xia et al. (2016) by province and sector to calculate PM emissions from 1985 to 1995. The PM_{10} emissions in 2000 were estimated at 15.6 Tg in Xia et al. (2016) but were 13.4 Tg in EDGAR. To provide consistency in the estimates of interannual emissions, we simply adjusted the EDGAR emissions for 1985–1995 with a correction factor (15.6/13.4) for all sectors. The mass fractions of BCs in PM (w in Eq. (1)) by province and sector were taken from our previous studies, which were based on a national investigation, and updates of coal quality, interprovincial coal transport, and chemical composition of industrial materials (Zhao et al., 2011; Zhu et al., 2004).

We allocated the annual BC emissions into a $1^\circ \times 1^\circ$ grid system that covered mainland China. Emissions by large point sources with clear addresses were assigned to the grids where they were located. Other industrial and residential sources were treated as area sources, and their emissions were allocated according to the spatial distribution of industrial gross domestic production and population, respectively.

2.2. Model description for simulation of BCs, S and N deposition

2.2.1. Multilayer eulerian model for BC deposition simulation

Since the commonly used CTMs do not include the module of BC deposition simulation, we applied a multilayer dynamic Eulerian model to simulate the BC deposition from 1985 to 2015 with a five-year interval. This model was developed by Duan et al. (2007) and used the BC emission inventory, meteorological parameters and simplified empirical constants to simulate the long-range transport and deposition of BCs. As shown in Fig. S1 in the supplement, the modeling domain was within 18°N-53°N and 73°E−134°E, with a horizontal resolution of $1^\circ \times 1^\circ$. Three vertical layers (1000, 850 and 500 hPa at the top) were set in the model.

Besides the anthropogenic emission inventory described in Section

2.1, the emission data from natural sources were taken from Zhu et al. (2004), with no interannual change assumed in this work. The total natural emissions were estimated at 2080 Gg yr^{-1} for the country. Meteorological parameters were taken from the ERA Interim Daily database released by the European Center for Medium-Range Weather Forecasts (ECMWF, 2011) and the Global Precipitation Climatology Project (NASA and ESSIC, 2018). Empirical constants, including dry deposition velocity (V_d) and local deposition coefficients for anthropogenic and natural sources, were obtained from Duan et al. (2007). To evaluate the reliability of this model, we compared the simulated annual wet Ca deposition with available observations (see Text Section 1 in the supplement for details).

2.2.2. The EMEP MSC-W model for S and N deposition simulation

According to the availability of gridded emission inventory with sufficient horizontal resolution, we applied a 3-D CTM EMEP MSC-W and simulated the annual S and N deposition from 2000 to 2015 with a five-year interval (i.e., 2000, 2005, 2010, and 2015). The Meteorological Synthesizing Center-West (MSC-W) in Oslo, Norway of European Monitoring and Evaluation Program (EMEP) has conducted sufficient simulations and proved its good applicability for simulating acid deposition (Jeričević et al., 2010; Simpson et al., 2012). The meteorological driving field was obtained from the Weather Research and Forecasting v3.9.1 (WRF) Model. As shown in Fig. S1, the modeling domain of WRF-EMEP ranges 16°N-49°N and 78°E−141°E, with a horizontal resolution of 27 × 27 km. Table S1 summarizes the physical and chemical scheme settings and input data of the model. We applied MEIC with an original horizontal resolution of 0.25° × 0.25° as the emission input. We used FNL meteorological data from the National Center for Environmental Prediction (NCEP and NOAA, 2000) with a horizontal resolution of 1° × 1° as the initial and boundary conditions of the meteorological field. The Global Land Cover 2015 (GLC) land-use data http://due.esrin.esa.int/page_globcover.phpfrom European Space Agency (ESA, 2017) were applied for the whole simulation period. We compared the simulated annual and monthly deposition with available observations to evaluate the model performance (see Text Section 1 for details).

2.3. The extended steady-state mass balance model for critical load (CL) mapping

The CL of S and N for terrestrial ecosystems can be calculated with Eqs. (2)–(4) based on an extended steady-state mass balance (SSMB) model (UNECE, 2004; Zhao et al., 2007; see Text Sections 2 and 3 and Fig. S2 in the supplement for details). This model links deposition to a chemical criterion and assumes that the formulation and depletion of acidity and alkalinity in soil are time-independent and simultaneously considers the changes in the deposition of S, N and BCs:

$$CL_{max}(S) = BC_D + BC_W - BC_U - ANC_{L,crit} \quad (2)$$

$$CL(N) = N_I + N_U + \frac{min(CL_{max}(S), N_{L,crit})}{1 - f_{DE}} \quad (3)$$

$$CL(S) = \begin{cases} CL_{max}(S) & (N_D \le N_I + N_U) \\ CL_{max}(S) - (1 - f_{DE})\,[N_D - (N_I + N_U)] & (N_D > N_I + N_U) \end{cases} \quad (4)$$

where $CL(S)$ and $CL(N)$ are the critical loads of S and N, respectively; BC_D is the deposition of BCs; BC_W is the weathering rate of BCs from soil minerals; BC_U and N_U are the vegetation uptakes of BCs and N, respectively; $ANC_{L,\ crit}$ is the critical leaching of alkalinity; N_I is the average immobilization rate of N in soil for a long period; $N_{L,crit}$ is the critical leaching flux of N; f_{DE} is the denitrification rate of N; and N_D is the deposition of N.

$ANC_{L,\ crit}$ in Eq. (2) was calculated with a critical limit $(Bc/Al)_{crit}$, which indicates the connection between soil chemical status and plant response (damage to fine root) via a critical molar ratio of the concentrations of base cations to aluminum in soil solution. $N_{L,crit}$ in Eq. (3) was calculated with a critical limit $[NO_3^-]_{crit}$, which indicates the acceptable concentration of leaching NO_3^- depending on the eutrophiciation damage that should be avoided (see Text Sections 2 and 3 and Table S2 in the supplement for details). The spatiotemporal patterns of BC_D were simulated as described in Section 2.2.1. Following the methods by Duan et al. (2002) and Duan et al. (2004), the spatial distributions of vegetation and soil parameters in Eqs. (2)–(4) were obtained at a horizontal resolution of 0.1° × 0.1° based on the comprehensive datasets of the national field investigations (IGSNRR, 2019). Those investigations were conducted every a few decades, thus the data reflected the average conditions of vegetation and soil for a relatively long-term period (internal communication with researcher in IGSNRR). The annual average temperatures were taken from the Resource and Environment Data Cloud Platform provided by the Institute of Geographic Sciences & Natural Resources Research, Chinese Academy of Sciences (IGSNRR, 2019). Due to the kinetic limitation of BC_W, we adopted the Arrhenius equation to quantify the interannual variations in BC_W due to changing temperatures:

$$BC_w = BC_{w0}\, e^{\left(\frac{A}{T_0} - \frac{A}{T}\right)} \quad (5)$$

where T_0 is the reference temperature (281 K), T is the actual temperature, BC_{w0} is the weathering rate at T_0 (Duan et al., 2002), and A is the Arrhenius pre-exponential factor (3600 K).

Exceedances of S ($Ex(S)$) and N ($Ex(N)$) were calculated by comparing the simulated deposition with CL for corresponding species from 2000 to 2015 with a five-year interval.

3. Results and discussions

3.1. The emissions and deposition of BCs

The annual anthropogenic BC (Ca and Mg) emissions from 1985 to 2015 are shown by sector in Fig. 1 (see the provincial emissions in Tables S3 and S4). In general, the emissions of both species were found to keep increasing until mid-2000, followed by a continuous decline afterward. A mismatch of BC emissions around 2000 needs to be noted even if we adjusted the 2 PM inventories. The smaller emissions in 2000 than 1995 and 2005 could result partly from the bias in energy statistics for that period. Based on the interannual variability in NO_2 column from satellite observation, Akimoto et al. (2006) implied an underestimation in the national total fuel consumption by Chinese Energy Statistics Yearbook during 1996–2000.

The total Ca emissions were estimated to increase from 4504 in 1985 to 5645 Giga grams (Gg) in 2005 and then decrease below the 1985 level to 3492 Gg in 2015. The Mg emissions increased from 238 Gg in 1985 to 371 Gg in 2005 and then decreased to 298 Gg in 2015. Cement and other industrial processes were identified as the dominant sources of Ca. The two sectors contributed 65 % and 28 % of the total national emissions for 2000, while the fractions were 25 % and 61 % in 2015, respectively (see the details in Table S5). The raw materials used in cement production (tricalcium silicate, tricalcium aluminate, and free calcium oxide) resulted in much larger mass fraction of Ca in PM emissions (28%–44 %) than other sources. Our estimates of BC emissions for 1995–2005 were −2% to −21 % lower than those of Lei et al. (2011), due to the uncertainty in activity data of small cement and lime plants.

The interannual variabilities in total BC emissions and their sector contributions resulted from the tremendous change in industrial structures, elevated penetration of improved manufacturing technology, and implementation of stricter PM emission controls (Zhang et al., 2019). For example, China gradually eliminated inefficient and small factories and tightened PM emission standards for cement plants from 50 to 30 mg m^{-3} in 2014 (Zheng et al., 2018). Old rotary and shaft kilns have been replaced with advanced precalciners with fabric filter dust

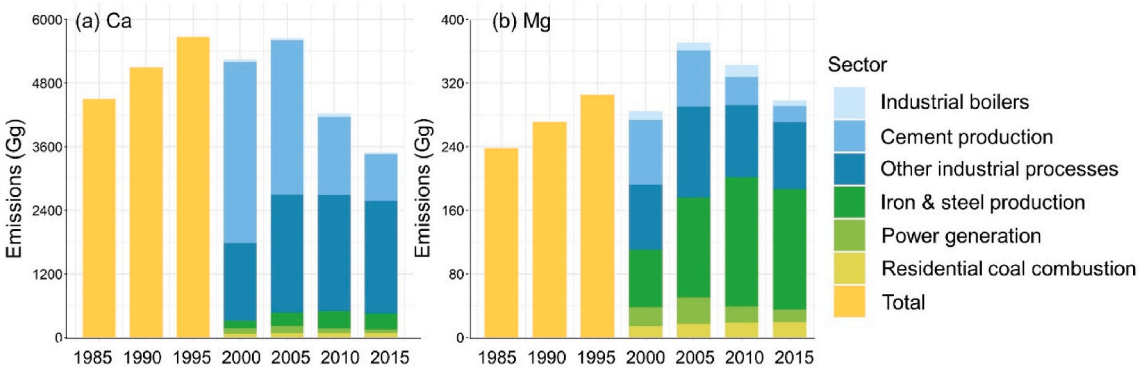

Fig. 1. The annual Ca and Mg emissions by sector in mainland China (1985–2015).

collectors (Li et al., 2017). These advanced technologies make rational use of raw materials and improve the removal efficiency of PM, resulting in significant reductions in Ca emissions. The spatial distributions of anthropogenic BC emissions are shown in Fig. S3. North and Southeast China accounted for over 70 % of the national anthropogenic BC emissions on average from 1985 to 2015, while Northwest China and the Tibetan Plateau accounted for less than 6 % (see the regional definition in Fig. S1). Due to the relatively high levels of industrialization and urbanization, the urban construction and industrial production in developed North and Southeast China produced abundant PM emissions and thereby BCs.

Fig. S4 compares the simulated and observed annual wet BC deposition at specific monitoring sites, and the normal mean biases (NMBs) and normalized mean errors (NMEs) ranged from −32 % to 21 % and from 39 % to 47 %, respectively, from 2000 to 2015 (Table S6). Basically, the model captured the spatial distributions of BC deposition for different years. It underestimated the deposition for earlier years but overestimated for the more recent ones. In general, the bias could result from the simplified atmospheric processes, coarse horizontal resolution of the model and the uncertainty in emission estimation. The model performance and the main reasons for the simulation bias are presented in details in Text Section 1 in the supplement.

Fig. 2 shows the interannual variations in spatial patterns of the simulated BC deposition from 1985 to 2015. Large BC deposition was clearly found in the north, southeast, and border of Xinjiang and Qinghai, while low deposition was in Tibet. Northwest, Southeast and North China contributed 25.3 %, 23.3 % and 20.0 % of BC deposition on average, respectively. Anthropogenic activities contributed most of the BC deposition in the developed North and Southeast China, while 79 % of total BC deposition in Northwest and Qinghai originated from natural dust. The deposition was above 0.3 keq ha^{-1} yr^{-1} for approximately one third of mainland China, while it varied between 0.1 and 0.3 keq ha^{-1} yr^{-1} in the U.S. in 2000s (Vet et al., 2014). The difference in deposition partly reflected the different development stages between the two countries. Due to earlier industrial development, the U.S. reached its peak in PM emissions in 1980s (Crippa et al., 2018; Klimont et al., 2017). The later accelerated industrialization and urbanization in China led to higher BC emissions and thereby deposition than the U.S. in early 2000s. As previously mentioned, clear reduction in emissions was found in following years over the country, resulting mainly from the improved industrial structure and PM controls (Li et al., 2017).

The total annual deposition over the country was simulated to

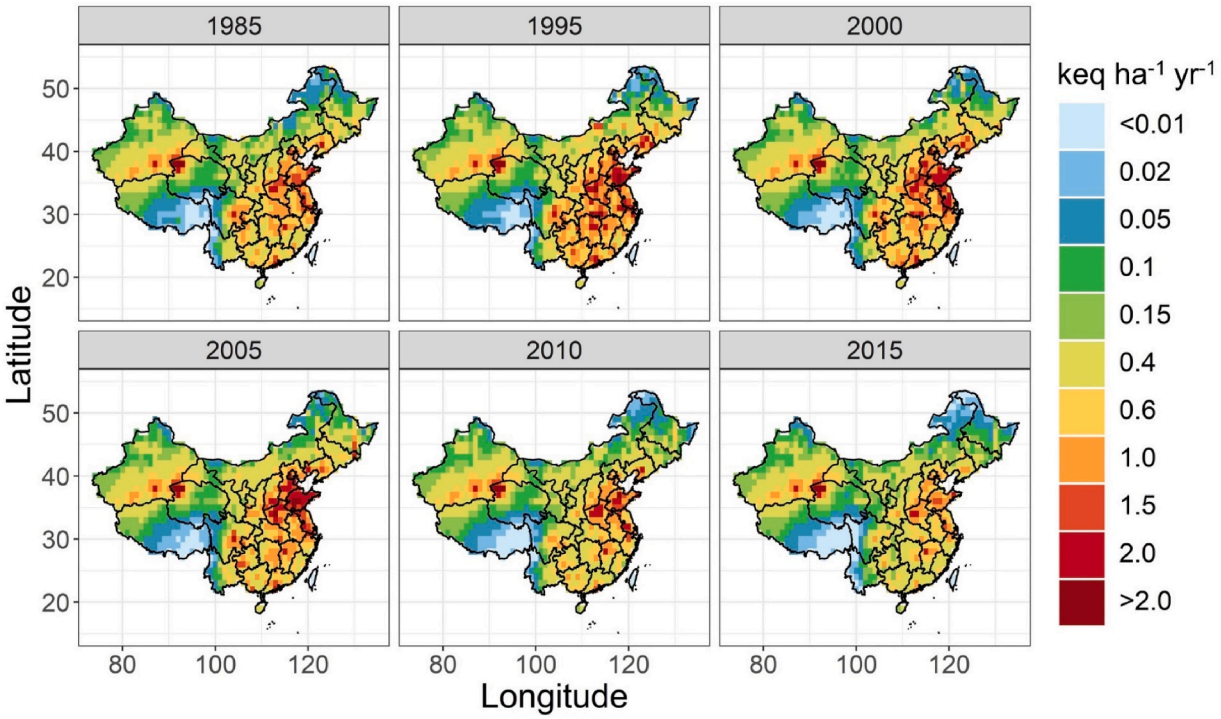

Fig. 2. The spatial distributions of BC (Ca + Mg) deposition in China (1985–2015). The horizontal resolution is 1° × 1°.

increase by 16 % in 1985–2005 and then be followed by a reduction of 32 % in 2005–2015. The temporal patterns of BC deposition varied by region. From 1985 to 2005, the growth in annual deposition was determined to be the largest for North China, at 52 %, followed by a reduction of 45 % from 2005 to 2015. For the southeast, as a comparison, deposition peaked in 1995 with a growth of 40 % from 1985 to 1995 and then declined by 53 % from 1995 to 2015. Overall, stricter environmental requirements of local governments and the shift from heavy industry to high-tech industries in developed provinces of Southeast China (e.g., Jiangsu, Zhejiang, Shanghai and Guangdong) have resulted in a decreasing PM pollution trend since the 1990s (Lei et al., 2011), while pollution continued to increase until 2007 in North China (Hu et al., 2010; Ma et al., 2019).

3.2. The updated CL mapping of S and N

Fig. S6 in the supplement illustrates the updated $CL_{max}(S)$ and $CL(N)$ mapping for China 2015. Large $CL_{max}(S)$ commonly appeared in Northwest China and the Tibetan Plateau, indicating relatively low acidification risks (Fig. S6a). The high weathering rates of BCs from arid environments and the abundant BC deposition from natural sources resulted in high alkalinity inputs, while the low vegetation uptake rate of BCs limited alkalinity outputs (Posch et al., 2015). The areas with low $CL_{max}(S)$ included Northeast, North, Southeast and Southwest China. The low $CL_{max}(S)$ in Northeast China resulted from the small BC weathering rates in cold weather and the strongly acidified soil (Duan et al., 2002). In Southwest and Southeast China, the vegetation mainly includes subtropical evergreen broad-leaved forests with a high uptake rate of BCs, leading to a weak capability of buffering acid deposition. $CL(N)$ presented an opposite spatial pattern compared to $CL_{max}(S)$. High $CL(N)$ appeared in Northeast, North, Southeast and Southwest China, and low in Northwest and Tibetan Plateau (Fig. S6b). Compared to southern China, the uptake and denitrification rate of N were lower in Northwest and Tibetan Plateau, attributable to the cold and dry climate, and abundance of deserts and grasslands.

Although the spatial patterns of CL in this study were of limited differences from previous (Duan et al., 2000; Posch et al., 2015), the latters ignored the effect of long-term change of alkalinity inputs on CL. Fig. 3 shows the differences in spatial patterns of $CL_{max}(S)$ and $CL(N)$ from 1985 to 2005 (the period with increased BC deposition) and those from 2005 to 2015 (the period with decreased BC deposition). The area with increased $CL_{max}(S)$ values accounted for 67 % of the entire country during 1985–2005 (Fig. 3a). The largest $CL_{max}(S)$ growth was estimated at 1.05, 0.98, and 0.96 keq ha^{-1} yr^{-1} for Henan, Beijing and Shandong respectively. The increased $CL_{max}(S)$ resulted partly from the elevated BC emissions and thereby deposition across the country. More significant changes were found for provinces with substantial growth in anthropogenic BC emissions, e.g., Shandong, with the annual emissions increased by 315 Gg. Moreover, the increased temperatures from 1985 to 2015 elevated alkalinity inputs from soil weathering, particularly in Northwest China. For example, the annual average temperature in Qinghai increased by 1.8 °C during this period, leading to an increase in $CL_{max}(S)$ of 0.37 keq ha^{-1} yr^{-1}.

From 2005 to 2015, the areas with a reduced $CL_{max}(S)$ accounted for 55 % of the entire country and were mainly distributed in Northwest, Southwest, North and Southeast China (Fig. 3b). The largest reduction in $CL_{max}(S)$ was found in Henan, Guangdong and Shandong, reaching 1.30, 0.99 and 0.92 keq ha^{-1} yr^{-1}, respectively. The reduced $CL_{max}(S)$ resulted mainly from the abatement of BC emissions. Shandong was the province with the largest Ca emission reduction (360 Gg) from 2005 to 2015. The reductions in Guangdong, Henan, and Zhejiang also exceeded 100 Gg. In contrast, increased $CL_{max}(S)$ values were found in Tibet, southern Inner Mongolia, and Guangxi. In less developed regions with fewer industrial sources, anthropogenic BC deposition was not the main

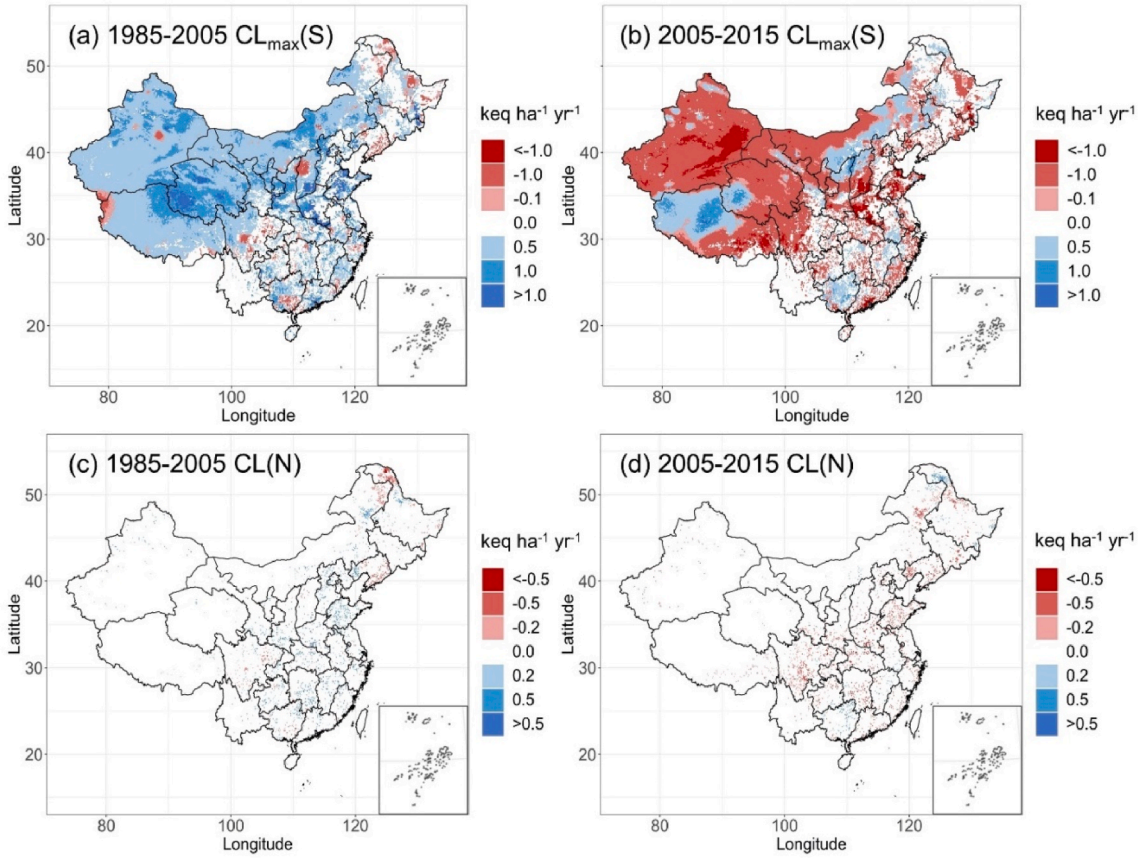

Fig. 3. The changes in $CL_{max}(S)$ and $CL(N)$ from 1985 to 2005 (a and c) and from 2005 to 2015 (b and d). The horizontal resolution is 0.1° × 0.1°.

contributor to soil alkalinity, and the variations in $CL_{max}(S)$ could be dominated by other factors. For example, the annual temperature in 2015 was higher than that in 2005 in most parts of Guangxi, resulting in elevated soil weathering rate and therefore increased alkalinity inputs. This could offset the effect of reduced BC deposition and increase the CL.

Fig. 3c and d presents the differences in $CL(N)$ for the two periods. $CL(N)$ was estimated to increase in 2.0 % of the whole country in 1985–2005 and to decrease in 2.8 % in 2005–2015. Over 95 % of the territory exhibited no interannual variability, as the uptake, immobilization, and denitrification of N were assumed to be unchanged in the $CL(N)$ calculation in this work.

3.3. The deposition of S and N and CL exceedances

The model performance of S and N deposition simulation with EMEP was presented in Text Section 1 in the supplement. As summarized in Table S6, in general, EMEP underestimated S and N deposition (particularly for reduced nitrogen, RDN), with NMBs and NMEs ranging from −60 % to 50 % and from 43 % to 96 %, respectively. Compared with the common simulation bias between −70 % and 800 % (Chang et al., 2020), the performance of EMEP was reasonable and representative of the spatiotemporal deposition patterns. Issues of model application, biases in emission inventories and fixed land-use data were expected to influence the simulation (see Text Section 1 for details).

Fig. S7 illustrates the interannual changes in spatial distributions of S and N deposition from 2000 to 2015. Similar to previous studies (Ge et al., 2020; Zhang et al., 2018b), a relatively large deposition was present in North, Southeast and Southwest China, attributed mainly to the high emissions from the developed agriculture and industry. In addition, the basin topography in Sichuan and Chongqing and the increased surface roughness due to urbanization in developed regions restrict pollutant diffusion and transport.

The temporal evolution of deposition differed between S and N. The annual total S deposition was estimated to increase by 49 % in 2000–2005, with a peak of 14.4 Mt in 2005, and then decreased by 17 % and 32 % in 2005–2010 and 2010–2015, respectively. The reduced S deposition could be caused by the strict emission control measures implemented since 2005, including FGD application in power generation and iron & steel production and improvement in industrial manufacturing technologies (Li et al., 2017). Moreover, the annual deposition was estimated to decrease more sharply from 2010 to 2015 by 32 % than that from 2005 to 2010 by 17 %, reflecting the greater benefit from SO_2 emission reduction after 2010. Much stricter emission standards for coal-fired power and industrial coal boilers have been issued since 2010, motivating the upgrading and improved operation of emission control facilities (MEP and GAQSIQ, 2011, 2014).

N deposition was estimated to increase by 32 % in 2000–2010, with a peak of 15.8 Mt in 2010, and a limited change was found afterward. NO_X controls were commonly conducted several years later than those for SO_2, e.g., the compulsory use of FGD in the power sector began after 2005, while that of SCR after 2010. Besides, very few controls have been implemented for agricultural NH_3 emissions (Liu et al., 2019). Consequently, as shown in Table S7, the ratio of RDN to oxidized nitrogen (OXN) deposition declined from 1.72 to 0.81 during 2000–2010 and increased again to 0.93 in 2015. In contrast to China, the ratio of RDN to OXN in the U.S. has increased from 0.72 to 1.49 during 1985–2012, resulting from the large reduction in NO_X emissions from industrial power generation (Du et al., 2014). In Europe, this ratio was found to increase from 1.10 in 1997 to 1.22 in 2005 (Simpson et al., 2006, 2014), attributed to relatively stable NH_3 emissions but continuously reduced NO_X since 1980 (Crippa et al., 2018). The various temporal trends of the ratio thus presented the different progresses of NO_X controls between the countries.

Fig. 4 illustrates the spatial patterns of the CL exceedance from 2000 to 2015, and Table 1 summarizes the annual total exceedances. The fractions of areas with $Ex(S)$ reached 52 %, 43 % and 31 % for Southwest, Northeast and Southeast China, respectively, while there was

Table 1
The exceedances of S and N critical loads in China with (base case) and without (hypothetical case) the interannual changes in BC deposition from 2000 to 2015 (unit: Mt).

		2000	2005	2010	2015
Base case	*Ex* (*S*)	2.92	4.63	3.90	2.48
	Ex (*N*)	0.40	0.65	1.21	1.06
Hypothetical case	*Ex* (*S*)	2.92	4.63	3.65	2.20
	Ex (*N*)	0.40	0.65	1.17	1.01

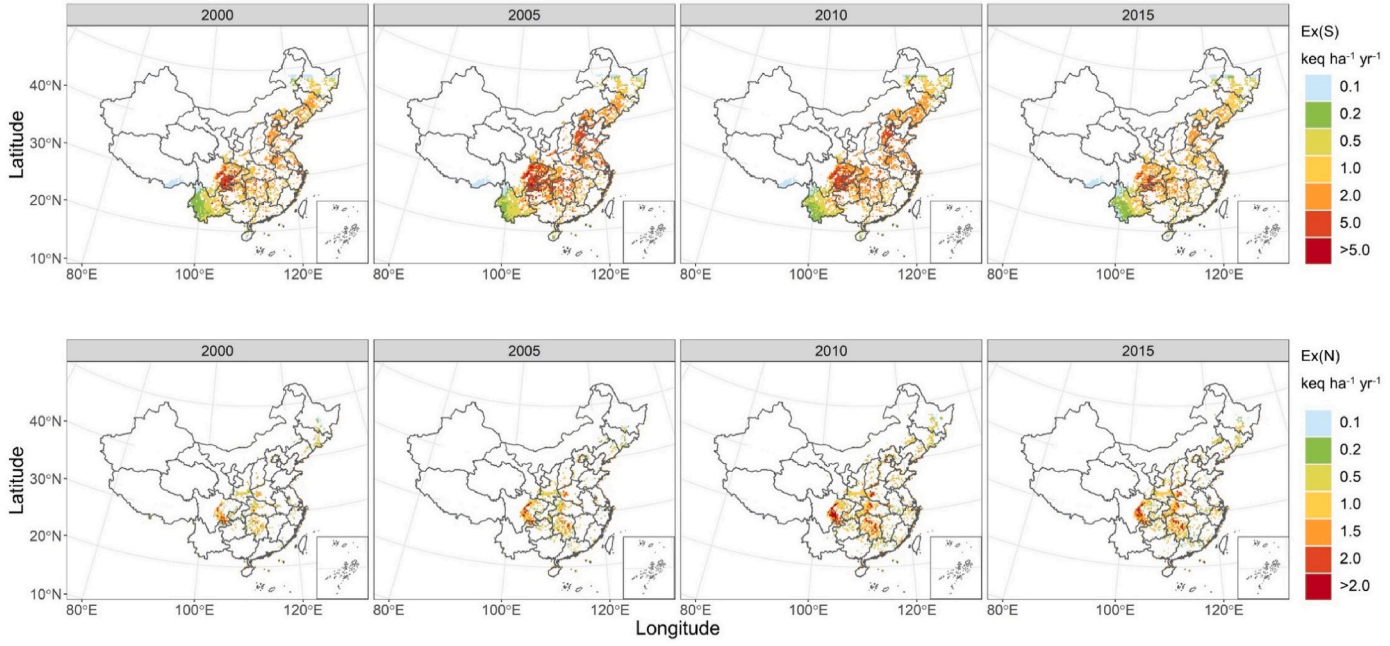

Fig. 4. The exceedances of S and N critical loads in mainland China (2000–2015). The horizontal resolution is 27 × 27 km.

nearly no *Ex*(*S*) in Northwest and Tibetan Plateau. The large SO_2 emissions from intensive coal burning resulted in high S deposition in the developed Southeast China and thus elevated the CL exceedance. For Southwest, the sulfur contents in coal were much higher than those in other regions, leading to substantial SO_2 emissions and *Ex*(*S*). From 2000 to 2005, *Ex*(*S*) over the entire country was estimated to increase from 2.9 to 4.6 Mt and then decrease 46 % to 2.5 Mt in 2015. The greatest change was found in North China, with a growth of 88 % during 2000–2005 and a reduction of 50 % during 2005–2015. The interannual changes in *Ex*(*S*) demonstrated the benefit of SO_2 control on reducing soil acidification after 2005. To evaluate the effect of BC deposition on CL exceedance, we further defined a hypothetical case in which BC deposition during 2005–2015 was assumed unchanged from the 2000 level. The case presented a situation in which PM emission controls had not been conducted since 2000. Based on this assumption, the *Ex*(*S*) levels in 2010 and 2015 would decrease by 0.25 and 0.28 Mt, i.e., 6.4 % and 11.2 % smaller than the base case with BC variability, respectively. The results suggested that the PM controls and consequent reduction in BC deposition moderately offset the decline of *Ex*(*S*) and delayed the soil acidification recovery. Given the underestimation in BC deposition for earlier years but overestimation for more recent years by our model, the reduced BC deposition and its impact on *Ex*(*S*) might be underestimated in 2000s. Besides, the ignorance of interannual change in natural dust deposition would lead to uncertainty in estimation of CL exceedance. As shown in Fig. 4, however, the region with high BC deposition from natural sources (Northwest) seldom had its CL exceeded. The reasons included the abundant alkalinity inputs from weathering and natural deposition, and the limited acid deposition due to small industrial emissions of gas precursors in the region. Therefore, the uncertainty should be moderate.

Ex(*N*) was mainly found in Southeast, Southwest and North China with relatively high deposition of N. Compared to S, *Ex*(*N*) was limited across the country since the areas receiving high N deposition also had a large *CL*(*N*) attributed to the considerable vegetation uptake of N. Consistent with the interannual trend of N deposition, *Ex*(*N*) increased from 0.40 in 2000 to 1.21 Mt in 2010 and then slightly decreased to 1.06 Mt in 2015. More significant increase in *Ex*(*N*) was found in specific regions, such as Sichuan and Chongqing. In the hypothetical case described above, the *Ex*(*N*) values for 2010 and 2015 were calculated to be 0.04 (3.6 %) and 0.05 Mt (5.0 %) smaller than the base case, respectively, reflecting the limited effect of BC variations on *Ex*(*N*). From 2000 to 2015, the net growth of *Ex*(*N*) was 165 % (0.66 Mt), and the reduction in BC deposition contributed 8 %. By combining the interannual changes in RDN and OXN deposition, the reduced *Ex*(*N*) during 2010–2015 resulted mainly from the declining OXN, while a relatively stable level was found for RDN.

In this study, the *Ex*(*S*) values for 2005 and 2010 (4.6 and 3.9 Mt, respectively) were close to those described in our previous work (4.1 and 3.8 Mt in Zhao et al. (2009)), while greater discrepancies were found for *Ex*(*N*) (0.65 and 1.21 Mt in this work and 2.76 and 4.19 Mt in Zhao et al. (2009), respectively). The much larger *Ex*(*N*) in Zhao et al. (2009) resulted from possible overestimation in NH_3 emissions and thereby N deposition, particularly for Inner Mongolia.

Comparison of the long-term trends in alkaline and acidic pollutant emissions and CL exceedances across the world could provide insights on the diversity in the progress and strategy of acidification risk mitigation between regions. Fig. S8 shows the relative changes in SO_2 and Ca emissions for China and the U.S. (PM_{10} as an indicator for Ca for the U.S. due to lack of exact data) during 1985–2015. More significant reduction in Ca (or PM_{10}) emissions compared to SO_2 was found in China than the U.S. at the decadal temporal scale, implying a bigger potential risk of ecosystem acidification for China. The US experienced a rising trend of CL exceedances until 1985, and the following decline suggested the effectiveness of the national policy on restraining the emissions of acid precursors (Clark et al., 2018; Sun et al., 2017). Observation on soil ion leaching revealed similar but hysteretic pattern of ecosystem response to the deposition (Gilliam et al., 2019). For Europe, N deposition was the main contributor to the CL exceedances, which peaked in 1980s and then declined due to economic transformation and emission abatement (Posch et al., 2015; Schmitz et al., 2019). As estimated in this work, China started to reduce its CL exceedance around 20 years behind U.S. and Europe, through mainly the tightened controls of SO_2. The different progresses between countries or regions reveal the impact of varied phases of economic development and air pollution controls on the ecosystem damage recovery. Although acknowledged by existing studies (Clark et al., 2018; Ellis et al., 2013; Makar et al., 2018; McDonnell et al., 2010), moreover, the effect of climate change on the historical trend in acidification risk was seldom quantified. Sun et al. (2017) reported a 38 % decline in CL exceedances in the U.S. due to the enhanced BC weathering from a 2 °C growth in temperature in 2050. With the national pollution control strategy gradually shifting from the end-of-pipe treatment to energy structure improvement in China, the impact of future climate change on ecological risk needs further careful investigation and evaluation.

4. Conclusions

We combined CTMs and CL to study the long-term impact of BCs, S, and N deposition on soil acidification in China. Driven mainly by the changed anthropogenic emissions, the annual deposition of BCs and S in China started to decline around 2005–2010, while that of N kept growing till 2010. The CL exceedance of S increased from 2.9 to 4.6 Mt during 2000–2005, and then decreased to 2.5 Mt in 2015, while that of N increased from 0.40 in 2000 to 1.2 Mt in 2010, with limited reduction afterward. The changes in CL exceedance matched the progress of national air pollution control for the past decade. Reduction in BC deposition from PM control moderately offset the benefit of SO_2 control on soil acidification recovery. The results highlighted the importance of a multi-pollutant control strategy for effectively reducing the ecological risk. In this work, the deposition relied on CTMs that simplified atmospheric processes, and discrepancies existed between observation and simulation for various species, years, and regions. More techniques are recommended for integrating available observation data and modeling results to better capture the long-term spatiotemporal patterns of atmospheric deposition of multiple species. Besides CL, moreover, multiple responses of plant biodiversity, soil microbial communities, and forest carbon and nitrogen cycling to atmospheric deposition are recommended to be further explored to help better understand the feedback of ecosystems to the changed deposition.

Author statement

Wenxin Zhao: Methodology, Investigation, Formal analysis, Data curation, Visualization, Software, Writing-Original draft preparation. **Yu Zhao:** Conceptualization, Methodology, Resources, Writing - Review & Editing. **Mingrui Ma:** Software. **Ming Chang:** Software. **Lei Duan:** Resources.

Declaration of competing interest

The authors declare that they have no known competing financial interests or personal relationships that could have appeared to influence the work reported in this paper.

Acknowledgements

This work was sponsored by the National Key Research and Development Program of China (2017YFC0210106) and the National Natural Science Foundation of China (41922052). We would like to thank Xuejun Liu from China Agricultural University for observed deposition data and Qiang Zhang from Tsinghua University for MEIC emission data.

Appendix A. Supplementary data

Supplementary data to this article can be found online at https://doi.org/10.1016/j.envpol.2021.117974.

References

Akimoto, H., Ohara, T., Kurokawa, J., Horii, N., 2006. Verification of energy consumption in China during 1996-2003 by using satellite observational data. Atmos. Environ. 40, 7663–7667.

Burns, D.A., Aherne, J., Gay, D.A., Lehmann, C.M.B., 2016. Acid rain and its environmental effects: recent scientific advances. Atmos. Environ. 146, 1–4.

Cecchini, G., Andreetta, A., Marchetto, A., Carnicelli, S., 2019. Atmospheric deposition control of soil acidification in central Italy. Catena 182, 104102.

Chang, M., Cao, J.C., Ma, M.R., Liu, Y.M., Liu, Y.Q., Chen, W.H., Fan, Q., Liao, W.H., Jia, S.G., Wang, X.M., 2020. Dry deposition of reactive nitrogen to different ecosystems across eastern China: a comparison of three community models. Sci. Total Environ. 720, 137548.

Clark, C.M., Phelan, J., Doraiswamy, P., Buckley, J., Cajka, J.C., Dennis, R.L., Lynch, J., Nolte, C.G., Spero, T.L., 2018. Atmospheric deposition and exceedances of critical loads from 1800-2025 for the conterminous United States. Ecol. Appl. 28, 978–1002.

Crippa, M., Guizzardi, D., Muntean, M., Schaaf, E., Dentener, F., van Aardenne, J.A., Monni, S., Doering, U., Olivier, J.G.J., Pagliari, V., Janssens-Maenhout, G., 2018. Gridded emissions of air pollutants for the period 1970-2012 within EDGAR v4.3.2. Earth Syst. Sci. Data 10, 1987–2013.

Draaijers, G.P.J., Van Leeuwen, E.P., De Jong, P.G.H., Erisman, J.W., 1997. Base cation deposition in Europe: part I. Model description, results and uncertainties. Atmos. Environ. 31, 4139–4157.

Du, E.Z., de Vries, W., Galloway, J.N., Hu, X.Y., Fang, J.Y., 2014. Changes in wet nitrogen deposition in the United States between 1985 and 2012. Environ. Res. Lett. 9, 095004.

Duan, L., Hao, J.M., Xie, S.D., Zhou, Z.P., Ye, X.M., 2002. Determining weathering rates of soils in China. Geoderma 110, 205–225.

Duan, L., Huang, Y., Hao, J., Xie, S., Hou, M., 2004. Vegetation uptake of nitrogen and base cations in China and its role in soil acidification. Sci. Total Environ. 330, 187–198.

Duan, L., Lin, Y., Zhu, X.Y., Tang, G.G., Gao, D.F., Hao, J.M., 2007. Modeling atmospheric transport and deposition of calcium in China. Tsinghua Univ. Sci. Technol. 47 (9), 1462–1465.

Duan, L., Xie, S.D., Zhou, Z.P., Hao, J.M., 2000. Critical loads of acid deposition on soil in China. Water, Air, Soil Pollut. 118, 35–51.

Ellis, R.A., Jacob, D.J., Sulprizio, M.P., Zhang, L., Holmes, C.D., Schichtel, B.A., Blett, T., Porter, E., Pardo, L.H., Lynch, J.A., 2013. Present and future nitrogen deposition to national parks in the United States: critical load exceedances. Atmos. Chem. Phys. 13, 9083–9095.

European Centre for Medium-range Weather Forecast (ECMWF), 2011. The ERA-interim reanalysis dataset, copernicus climate change service (C3S). available from: https://www.ecmwf.int/en/forecasts/datasets/archive-datasets/reanalysis-datasets/era-interim. (Accessed 10 April 2019). Accessed.

European Space Agency (ESA), 2017. Global Land Cover 2015 Land-Use Data available from: http://maps.elie.ucl.ac.be/CCI/viewer/download.php. (Accessed 12 March 2020). Accessed.

Fenn, M.E., Bytnerowicz, A., Schilling, S.L., Ross, C.S., 2015. Atmospheric deposition of nitrogen, sulfur and base cations in jack pine stands in the Athabasca Oil Sands Region, Alberta, Canada. Environ. Pollut. 196, 497–510.

Fu, H., Luo, Z., Hu, S., 2020. A temporal-spatial analysis and future trends of ammonia emissions in China. Sci. Total Environ. 731, 138897.

Ge, B., Itahashi, S., Sato, K., Xu, D., Wang, J., Fan, F., Tan, Q., Fu, J.S., Wang, X., Yamaji, K., Nagashima, T., Li, J., Kajino, M., Liao, H., Zhang, M., Wang, Z., Li, M., Woo, J.-H., Kurokawa, J., Pan, Y., Wu, Q., Liu, X., Wang, Z., 2020. Model Inter-Comparison Study for Asia (MICS-Asia) phase III: multimodel comparison of reactive nitrogen deposition over China. Atmos. Chem. Phys. 20, 10587–10610.

Gilliam, F.S., Burns, D.A., Driscoll, C.T., Frey, S.D., Lovett, G.M., Watmough, S.A., 2019. Decreased atmospheric nitrogen deposition in eastern North America: predicted responses of forest ecosystems. Environ. Pollut. 244, 560–574.

Hettelingh, J.-P., Posch, M., Velders, J.M., Ruyssenaars, P., Adam, M., de Leeuw, F., Lükewille, A., Maas, R., Sliggers, J., Slootweg, J., 2013. Assessing interim objectives for acidification, eutrophication and ground-level ozone of the EU National Emissions Ceilings Directive with 2001 and 2012 knowledge. Atmos. Environ. 75, 129–140.

Hu, H., Yang, Q., Lu, X., Wang, W.C., Wang, S.S., Fan, M.H., 2010. Air pollution and control in different areas of China. Crit. Rev. Environ. Sci. Technol. 40, 452–518.

Institute of Geographic Sciences and Natural Resources Research, Chinese Academy of Sciences (IGSNRR), 2019. Spatial Interpolation Dataset of Annual Mean Temperature in China since 1980 available from: http://www.resdc.cn. (Accessed 3 April 2019). Accessed.

Jeričević, A., Kraljević, L., Grisogono, B., Fagerli, H., Večenaj, Ž., 2010. Parameterization of vertical diffusion and the atmospheric boundary layer height determination in the EMEP model. Atmos. Chem. Phys. 10, 341–364.

Jeziorski, A., Smol, J.P., 2017. The ecological impacts of lakewater calcium decline on softwater boreal ecosystems. Environ. Rev. 25, 245–253.

Jia, J.J., Gao, Y., 2017. Acid deposition and assessment of its critical load for the environmental health of waterbodies in a subtropical watershed, China. J. Hydrol. 555, 155–168.

Klimont, Z., Kupiainen, K., Heyes, C., Purohit, P., Cofala, J., Rafaj, P., Borken-Kleefeld, J., Schopp, W., 2017. Global anthropogenic emissions of particulate matter including black carbon. Atmos. Chem. Phys. 17, 8681–8723.

Larssen, T., Carmichael, G.R., 2000. Acid rain and acidification in China: the importance of base cation deposition. Environ. Pollut. 110, 89–102.

Lei, Y., Zhang, Q., He, K.B., Streets, D.G., 2011. Primary anthropogenic aerosol emission trends for China, 1990-2005. Atmos. Chem. Phys. 11, 931–954.

Li, M., Liu, H., Geng, G.N., Hong, C.P., Liu, F., Song, Y., Tong, D., Zheng, B., Cui, H.Y., Man, H.Y., Zhang, Q., He, K.B., 2017. Anthropogenic emission inventories in China: a review. Natl. Sci. Rev. 4, 834–866.

Liu, F., Zhang, Q., Tong, D., Zheng, B., Li, M., Huo, H., He, K.B., 2015. High-resolution inventory of technologies, activities, and emissions of coal-fired power plants in China from 1990 to 2010. Atmos. Chem. Phys. 15, 13299–13317.

Liu, M., Huang, X., Song, Y., Tang, J., Cao, J., Zhang, X., Zhang, Q., Wang, S., Xu, T., Kang, L., Cai, X., Zhang, H., Yang, F., Wang, H., Yu, J.Z., Lau, A.K.H., He, L., Huang, X., Duan, L., Ding, A., Xue, L., Gao, J., Liu, B., Zhu, T., 2019. Ammonia emission control in China would mitigate haze pollution and nitrogen deposition, but worsen acid rain. Proc. Natl. Acad. Sci. Unit. States Am. 116, 7760–7765.

Ma, Z., Liu, R., Liu, Y., Bi, J., 2019. Effects of air pollution control policies on $PM_{2.5}$ pollution improvement in China from 2005 to 2017: a satellite-based perspective. Atmos. Chem. Phys. 19, 6861–6877.

Makar, P.A., Akingunola, A., Aherne, J., Cole, A.S., Aklilu, Y.-a., Zhang, J., Wong, I., Hayden, K., Li, S.-M., Kirk, J., Scott, K., Moran, M.D., Robichaud, A., Cathcart, H., Baratzedah, P., Pabla, B., Cheung, P., Zheng, Q., Jeffries, D.S., 2018. Estimates of exceedances of critical loads for acidifying deposition in Alberta and Saskatchewan. Atmos. Chem. Phys. 18, 9897–9927.

McDonnell, T.C., Cosby, B.J., Sullivan, T.J., McNulty, S.G., Cohen, E.C., 2010. Comparison among model estimates of critical loads of acidic deposition using different sources and scales of input data. Environ. Pollut. 158, 2934–2939.

McHale, M.R., Burns, D.A., Siemion, J., Antidormi, M.R., 2017. The response of soil and stream chemistry to decreases in acid deposition in the Catskill Mountains, New York, USA. Environ. Pollut. 229, 607–620.

Meesenburg, H., Ahrends, B., Fleck, S., Wagner, M., Fortmann, H., Scheler, B., Klinck, U., Dammann, I., Eichhorn, J., Mindrup, M., Meiwes, K.J., 2016. Long-term changes of ecosystem services at Solling, Germany: recovery from acidification, but increasing nitrogen saturation? Ecol. Indicat. 65, 103–112.

Mesoscale Atmospheric Processes Branch, 2018. Laboratory for Atmospheres, Earth Sciences Division, Science and Exploration Directorate, Goddard Space Flight Center, NASA (NASA), and Earth System Science Interdisciplinary Center, University of Maryland (ESSIC). https://doi.org/10.5065/PV8B-HV76. GPCP Version 1.3 One-Degree Daily Precipitation Data Set, Research Data Archive at the National Center for Atmospheric Research, Computational and Information Systems Laboratory, available from: (Accessed 10 April 2019). Accessed.

Ministry of Ecology and Environment of China (MEE), 2020. Official Report on the State of the Environment available from: http://www.mee.gov.cn/hjzl/sthjzk/sthjtjnb/. (Accessed 19 April 2021). Accessed.

Ministry of Environment Protection of China (MEP) and General Administration of Quality Supervision, Inspection and Quarantine of China (GAQSIQ), 2011. Emission Standard of Air Pollutants for Thermal Power Plants. GB 13223-2011. China Environmental Science Press, Beijing, China.

Ministry of Environment Protection of China (MEP) and General Administration of Quality Supervision, Inspection and Quarantine of China (GAQSIQ), 2014. Emission Standard of Air Pollutants for Boiler. GB 13271-2014. China Environmental Science Press, Beijing, China.

Nanus, L., Clow, D.W., Saros, J.E., Stephens, V.C., Campbell, D.H., 2012. Mapping critical loads of nitrogen deposition for aquatic ecosystems in the Rocky Mountains, USA. Environ. Pollut. 166, 125–135.

National Centers for Environmental Prediction (NCEP), 2000. National weather service, NOAA, U.S (NOAA). Department of commerce. continuing from July 1999, Research Data Archive at the National Center for Atmospheric Research NCEP FNL Operational Model Global Tropospheric Analyses. Computational and Information Systems Laboratory. https://doi.org/10.5065/D6M043C6. available from: (Accessed 12 March 2020).

Pardo, L.H., Fenn, M.E., Goodale, C.L., Geiser, L.H., Driscoll, C.T., Allen, E.B., Baron, J.S., Bobbink, R., Bowman, W.D., Clark, C.M., Emmett, B., Gilliam, F.S., Greaver, T.L., Hall, S.J., Lilleskov, E.A., Liu, L.L., Lynch, J.A., Nadelhoffer, K.J., Perakis, S.S., Robin-Abbott, M.J., Stoddard, J.L., Weathers, K.C., Dennis, R.L., 2011. Effects of nitrogen deposition and empirical nitrogen critical loads for ecoregions of the United States. Ecol. Appl. 21, 3049–3082.

Payne, R.J., Stevens, C.J., Dise, N.B., Gowing, D.J., Pilkington, M.G., Phoenix, G.K., Emmett, B.A., Ashmore, M.R., 2011. Impacts of atmospheric pollution on the plant communities of British acid grasslands. Environ. Pollut. 159, 2602–2608.

Posch, M., Duan, L., Reinds, G.J., Zhao, Y., 2015. Critical loads of nitrogen and sulphur to avert acidification and eutrophication in Europe and China. Landsc. Ecol. 30, 487–499.

Reinds, G.J., Posch, M., De Vries, W., Slootweg, J., Hettelingh, J.-P., 2008. Critical loads of sulphur and nitrogen for terrestrial ecosystems in Europe and northern Asia using different soil chemical criteria. Water, Air, Soil Pollut. 193, 269–287.

Reis, S., Grennfelt, P., Klimont, Z., Amann, M., ApSimon, H., Hettelingh, J.-P., Holland, M., Le-Gall, A.-C., Maas, R., Posch, M., Spranger, T., Sutton, M.A., Williams, M., 2012. From acid rain to climate change. Science 338, 1153–1154.

Schmitz, A., Sanders, T.G.M., Bolte, A., Bussotti, F., Dirnbock, T., Johnson, J., Penuelas, J., Pollastrini, M., Prescher, A.K., Sardans, J., Verstraeten, A., de Vries, W., 2019. Responses of forest ecosystems in Europe to decreasing nitrogen deposition. Environ. Pollut. 244, 980–994.

Simpson, D., Andersson, C., Christensen, J.H., Engardt, M., Geels, C., Nyiri, A., Posch, M., Soares, J., Sofiev, M., Wind, P., Langner, J., 2014. Impacts of climate and emission changes on nitrogen deposition in Europe: a multi-model study. Atmos. Chem. Phys. 14, 6995–7017.

Simpson, D., Benedictow, A., Berge, H., Bergström, R., Emberson, L.D., Fagerli, H., Flechard, C.R., Hayman, G.D., Gauss, M., Jonson, J.E., Jenkin, M.E., Nyíri, A., Richter, C., Semeena, V.S., Tsyro, S., Tuovinen, J.P., Valdebenito, Á., Wind, P., 2012. The EMEP MSC-W chemical transport model – technical description. Atmos. Chem. Phys. 12, 7825–7865.

Simpson, D., Fagerli, H., Hellsten, S., Knulst, J.C., Westling, O., 2006. Comparison of modelled and monitored deposition fluxes of sulphur and nitrogen to ICP-forest sites in Europe. Biogeosciences 3, 337–355.

Sun, J., Fu, J.S., Lynch, J.A., Huang, K., Gao, Y., 2017. Climate-driven exceedance of total (wet plus dry) nitrogen (N) plus sulfur (S) deposition to forest soil over the conterminous US. Earths Fut. 5, 560–576.

United Nations Economic Commission for Europe (UNECE), 2004. Manual on Methodologies and Criteria for Modelling and Mapping Critical Loads and Levels and Air Pollution Effects, Risks and Trends available from: https://www.umweltbundesamt.de/en/manual-for-modelling-mapping-critical-loads-levels?parent=68093. (Accessed 17 January 2021). Accessed.

Vet, R., Artz, R.S., Carou, S., Shaw, M., Ro, C.-U., Aas, W., Baker, A., Bowersox, V.C., Dentener, F., Galy-Lacaux, C., Hou, A., Pienaar, J.J., Gillett, R., Forti, M.C., Gromov, S., Hara, H., Khodzher, T., Mahowald, N.M., Nickovic, S., Rao, P.S.P., Reid, N.W., 2014. A global assessment of precipitation chemistry and deposition of sulfur, nitrogen, sea salt, base cations, organic acids, acidity and pH, and phosphorus. Atmos. Environ. 93, 3–100.

Xia, Y.M., Zhao, Y., Nielsen, C.P., 2016. Benefits of of China's efforts in gaseous pollutant control indicated by the bottom-up emissions and satellite observations 2000-2014. Atmos. Environ. 136, 43–53.

Yu, H., He, N., Wang, Q., Zhu, J., Gao, Y., Zhang, Y., Jia, Y., Yu, G., 2017. Development of atmospheric acid deposition in China from the 1990s to the 2010s. Environ. Pollut. 231, 182–190.

Yu, Z.P., Chen, H.Y.H., Searle, E.B., Sardans, J., Ciais, P., Penuelas, J., Huang, Z.Q., 2020. Whole soil acidification and base cation reduction across subtropical China. Geoderma 361, 114107.

Zhang, Q., Zheng, Y., Tong, D., Shao, M., Wang, S., Zhang, Y., Xu, X., Wang, J., He, H., Liu, W., Ding, Y., Lei, Y., Li, J., Wang, Z., Zhang, X., Wang, Y., Cheng, J., Liu, Y., Shi, Q., Yan, L., Geng, G., Hong, C., Li, M., Liu, F., Zheng, B., Cao, J., Ding, A., Gao, J., Fu, Q., Huo, J., Liu, B., Liu, Z., Yang, F., He, K., Hao, J., 2019. Drivers of improved $PM_{2.5}$ air quality in China from 2013 to 2017. Proc. Natl. Acad. Sci. Unit. States Am. 116, 24463–24469.

Zhang, Q.Y., Wang, Q.F., Zhu, J.X., Xu, L., Chen, Z., Xiao, J.F., He, N.P., 2020. Spatiotemporal variability, source apportionment, and acid-neutralizing capacity of atmospheric wet base-cation deposition in China. Environ. Pollut. 262, 114335.

Zhang, T.A., Chen, H.Y.H., Ruan, H., 2018a. Global negative effects of nitrogen deposition on soil microbes. ISME J. 12, 1817–1825.

Zhang, X.Y., Chuai, X.W., Liu, L., Zhang, W.T., Lu, X.H., Zhao, L.M., Chen, D.M., 2018b. Decadal trends in wet sulfur deposition in China estimated from OMI SO_2 columns. J. Geophys. Res.-Atmos. 123, 10796–10811.

Zhao, Y., Duan, L., Larssen, T., Hu, L.H., Hao, J.M., 2007. Simultaneous assessment of deposition effects of base cations, sulfur, and nitrogen using an extended critical load function for acidification. Environ. Sci. Technol. 41, 1815–1820.

Zhao, Y., Duan, L., Lei, Y., Xing, J., Nielsen, C.P., Hao, J., 2011. Will PM control undermine China's efforts to reduce soil acidification? Environ. Pollut. 159, 2726–2732.

Zhao, Y., Duan, L., Xing, J., Larssen, T., Nielsen, C.P., Hao, J.M., 2009. Soil acidification in China: is controlling SO_2 emissions enough? Environ. Sci. Technol. 43, 8021–8026.

Zheng, B., Tong, D., Li, M., Liu, F., Hong, C., Geng, G., Li, H., Li, X., Peng, L., Qi, J., Yan, L., Zhang, Y., Zhao, H., Zheng, Y., He, K., Zhang, Q., 2018. Trends in China's anthropogenic emissions since 2010 as the consequence of clean air actions. Atmos. Chem. Phys. 18, 14095–14111.

Zhu, X., Duan, L., Tang, G., Hao, J., Dong, Y., 2004. Estimation of atmospheric emissions of base cations in China. J. Tsinghua Univ. (Sci. Technol.) 44, 1176–1179.